Progress in Engineering Science 3 (2026) 100378

Contents lists available at ScienceDirect

Progress in Engineering Science

journal homepage: www.sciencedirect.com/journal/progress-in-engineering-science

Effect of spray distance in D-gun sprayed Cr_3C_2–NiCr coatings on DSS 2205 in acidic environments

Roshan Kuruvila [a], Mebin T. Kuruvila [b], Manu Harilal [b], S. Thirumalai Kumaran [c,*]

[a] Department of Mechanical Engineering, Amal Jyothi College of Engineering, Kanjirapally, Kerala, 686518, India
[b] Department of Metallurgical & Materials Engineering, Amal Jyothi College of Engineering, Kanjirapally, Kerala, 686518, India
[c] Department of Mechanical Engineering, PSG Institute of Technology and Applied Research, Coimbatore, Tamil Nadu, 641062, India

ARTICLE INFO

Keywords:
Detonation gun spray
Corrosion
DSS
Acidic
Cr_3C_2-NiCr coating

ABSTRACT

Cermet coating, which is a blend of ceramic hardness and metallic toughness, is mostly applied to enhance the wear and corrosion resistance of metals. Detonation gun (D-gun) spraying is one of the most promising thermal spray technologies that would produce a high-quality ceramic coating. Cr_3C_2-NiCr coating is acceptable because of its superior mechanical characteristics and corrosion characteristic. The effectiveness of D-gun sprayed Cr_3C_2–NiCr coatings was evaluated under aggressive acidic conditions using 1 M H_2SO_4, which serves as a standardized laboratory electrolyte for assessing corrosion resistance relevant to industrial acidic environments, including the key process variables such as spraying distance, which is critically important in the determination of other coating properties such as porosity, adhesion, roughness, and hardness. Duplex stainless steel (DSS) 2205 has been sprayed with Cr_3C_2-NiCr at three spraying distances; 170 mm, 180 mm and 190 mm in an attempt to conduct the research on the behavior of Cr_3C_2-NiCr in acid conditions. Electrochemical activity of the coating was evaluated in 1 M H_2SO_4 solutions at room temperature; by open circuit potential (OCP), electrochemical impedance spectroscopy and potentiodynamic polarisation. Investigation of surface morphology under SEM revealed dense lamellar coatings with porosity decreasing from 2.84% at 170 mm to 1.38% at 190 mm, indicating improved particle melting and coating compactness. The coating deposited at 190 mm exhibited the best electrochemical performance, with lowest corrosion rate (0.113 mmpy), compared with the uncoated substrate (2.60 mmpy). All coated specimens had a homogenous and compact coating structure. The results demonstrate that 190 mm is the optimum spray distance for producing high-integrity Cr_3C_2–NiCr coatings on DSS 2205, providing enhanced corrosion protection for components operating in aggressive acidic industrial environments. This work demonstrates that optimizing the D-gun spray distance significantly influences the microstructural integrity and electrochemical corrosion behaviour of Cr_3C_2–25NiCr coatings on DSS 2205. The established processing–microstructure–performance relationship provides a scientific basis for optimizing D-gun coating parameters to enhance corrosion resistance in aggressive acidic environments.

1. Introduction

Acidic degradation in silicon-processing industries remains a significant challenge due to the aggressive nature of silicon-containing chemical environments, which accelerate material deterioration and compromise structural integrity. Corrosion challenges in silicon-based chemical plants are particularly severe in process units exposed to acidic media, leading to reduced service life and increased maintenance costs. Although Duplex Stainless Steel (DSS) 2205 offers excellent mechanical strength and moderate corrosion resistance, its application in highly acidic silicon-processing conditions is very critical and demands additional protection. Therefore, protective coatings for equipment handling silicon-containing chemicals have become essential to enhance surface durability, minimize material loss, and ensure long-term operational reliability in such harsh industrial environments.

In the oil and gas sector, pipelines are seen to be the most economical and effective means of transporting fluids. However, because of the nature of the fluids being conveyed and the harsh operating environments, pipeline systems are very susceptible to corrosion and mechanical damage [1–4], making strong mechanical durability a vital part of continuous work. However, Long-term exposure to corrosive media results in surface deterioration, subpar performance, and an increased risk

* Corresponding author.
E-mail address: thirumalaikumaran@psgitech.ac.in (S.T. Kumaran).

https://doi.org/10.1016/j.pes.2026.100378
Received 30 April 2026; Received in revised form 14 September 2026; Accepted 18 September 2026
Available online 21 September 2026
2950-4252/© 2026 Elsevier B.V. All rights are reserved, including those for text and data mining, AI training, and similar technologies.

of failure.

Therefore, it is necessary to develop superior materials, such as alloys, superalloys, composites, and protective coatings, that can affordably offer the necessary enhanced corrosion protection to improve the dependability and service life of equipments operating under harsh conditions. A unique blend of robust mechanical strength and corrosion resistance in materials is required in the extremely demanding service environment of oil and gas exploration and production.

DSS 2205 has emerged as a very promising alternative to conventional stainless steels in order to reduce the risks of failures that are typified by corrosions, financial losses, and safety problems. Because of its greater mechanical capacity and resistance to corrosion, it is also extensively utilized in offshore platforms, bridges, and coastal infrastructure [5–10]. Compared to single phase ferritic or austenitic alloys, the microstructure of DSS 2205, a blend of roughly equal proportions of austenite and ferrite, offers synergistic advantages such as greater strength, improved toughness, resistance to localized corrosion, and stress corrosion cracking [11–13]. With more than 35 years of successful service in the oil and gas industries, DSS has established itself as a material that can be relied upon to provide long-term structural integrity and safety by demonstrating its exceptional durability even under the harsh conditions of operation [14].

The production of a dense and stable oxide passive coating that acts as a barrier to aggressive media is primarily responsible for the corrosion resistance of DSS 2205 [15–17]. High concentrations of carbon dioxide, sulfides, and chlorides in crude oil have also been identified as some of the main causes of pipeline deterioration [18,19]. Therefore, it is crucial to investigate metallurgical methods that would reduce the corrosion susceptibility of these materials. These procedures include altering the material through metallurgical, mechanical, physical, or chemical treatments and applying sophisticated protective coating formulas that lessen surface deterioration [20–23]. The success of surface engineering solutions is significantly impacted by factors such as material and coating compatibility, functional performance requirements, adhesion strength, cost, and processing equipment accessibility. Thermal spray is a broad surface engineering technique that involves spraying a melted or semi-melted substance onto a surface to apply coatings. Because of its adaptability in improving the performance and service life of parts subjected to unfavorable operating circumstances, it can be widely used in any industry.

Thermal spray surfaces provide significant improvements in mechanical stability, thermal and chemical durability, and corrosion and wear resistance in both static and dynamic environments [24]. Steel and aluminum alloys' surface properties can be changed and strengthened using a variety of thermal spray techniques, such as high-velocity oxygen fuel (HVOF), plasma spraying, cold spraying, plasma electrolytic oxidation, and detonation gun (D-gun) coating. The specific application requirements, such as the required coating qualities, service circumstances, and cost considerations, determine the various benefits and drawbacks of these methods [25].

Among the available thermal spray technologies, cold spray and HVOF spraying have attracted considerable attention as alternative surface engineering processes for corrosion-resistant carbide-based coatings. Cold spray employs high-velocity solid-state particle deposition, thereby minimizing oxidation, phase transformation, and thermal degradation while producing dense coatings with excellent substrate adhesion. HVOF spraying, on the other hand, utilizes supersonic combustion gases to generate coatings with low porosity, high bond strength, and superior wear and corrosion resistance, making it one of the most widely adopted techniques for depositing Cr_3C_2–NiCr cermet coatings. Despite these advantages, detonation gun (D-gun) spraying is capable of imparting even higher particle velocities and producing exceptionally dense coatings with minimal oxide formation and improved interlamellar bonding. However, the influence of D-gun spray distance on the electrochemical corrosion behavior of Cr_3C_2–NiCr coatings deposited on DSS 2205 remains insufficiently understood. Therefore, the present study focuses on optimizing this critical processing parameter and comparing its influence on coating integrity and corrosion performance. [26]

One of the most effective thermal spray techniques for creating dense coatings with less than 1% porosity, low oxidation, and strong adhesion is D-gun coating. The high particle velocity, low operating temperature, ability to utilize a range of coating materials, and ability to adjust the process to provide a desired surface quality are some of the technology's many advantages over previous methods. The D-gun process works by feeding powder and a blended flammable gas mixture (such as acetylene and oxygen) into a closed barrel and using a spark plug to ignite them. The resulting shockwave then spreads to a high pressure, accelerating the powder particles to supersonic speeds. This causes the particles to contact the substrate and adhere firmly, creating a dense, sticky covering. When it comes to difficult industrial applications, D-gun spraying is highly preferred due to its high microstructural integrity and corrosion resistance [27–29].

Studies have shown that cermet coatings based on carbides are more resistant to corrosion, wear, and erosion than other alloys. The most popular carbide reinforcements, such chromium carbide (Cr_3C_2) and tungsten carbide (WC), are typically added to metal binders with Co, CoCr, or NiCr matrices, where the hardened carbide grains offer strength and hardness. Particularly in marine environments, coatings like WC-Co, WC- Co- Cr, and Cr_3C_2 -NiCr are currently being investigated as advantageous environmentally acceptable substitutes for conventional chromate-based coatings [28–31]. Carbide-based cermet coating has proven to be a reliable way to extend the lifespan of engineering products by stabilizing their service life and lowering maintenance expenses. Cr_3C_2-NiCr coatings were selected to be applied to DSS 2205 substrate using the D-gun technique based on these findings and filling in the knowledge gaps in the current literature. Additionally, Mudgal et al. verified that the chromium oxide and $NiCr_2O_3$ compounds that contribute to their improved corrosion resistance capabilities are formed by D-gun sprayed Cr_3C_2-$NiCr_2O$ coating [32,33].

Although Cr_3C_2–25NiCr coatings deposited by HVOF and plasma spraying have been extensively studied, the impact of D-gun spray distance on the microstructural evolution and electrochemical corrosion behavior of coatings deposited on DSS substrates has received less attention. Furthermore, there is a lack of comprehensive knowledge regarding the relationship between electrochemical performance, coating porosity, and spray distance.

Though many studies have examined the use of D-gun sprayed cermet on steel alloys to achieve higher levels of protection, none of the previous research has documented its application on DSS 2205. Since process parameters have a major influence on the protective performance of thermally sprayed coatings in harsh environments, it is imperative to precisely understand how these attributes are affected.

Therefore, the current study attempts to establish relationship between D-gun spray distance, coating porosity, and electrochemical corrosion resistance of Cr_3C_2-NiCr coatings deposited on DSS with spray distances of 170, 180, and 190 mm. The study determines the best processing conditions for enhancing the corrosion resistance of duplex stainless steel and establishes the correlation between D-gun spray distance and coating efficacy. It is demonstrated that this coating type can be utilized in conjunction with other coating types to give efficient corrosion resistance solutions under challenging service conditions.

2. Materials and methods

The graphical abstract presented in Fig. 1 shows the overall workflow and key outcomes of the study in a concise visual format. It illustrates the D-gun coating process, optimization of spray distance, characterization techniques, electrochemical testing, and the resulting improvement in the corrosion resistance of Cr_3C_2–25NiCr coated DSS 2205.

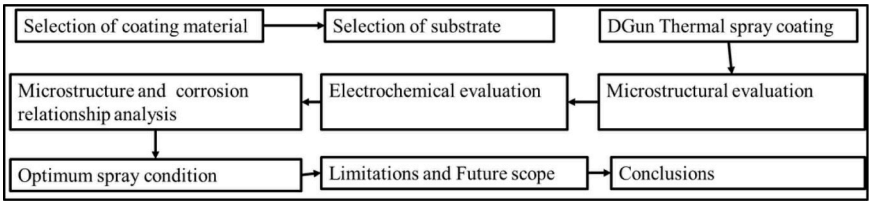


Fig. 1. Schematic representation of the study.

2.1. Fabrication of D-gun coatings

The substrate material for this study was a 5-mm-thick rectangular DSS 2205 plate [Fe-66.06%, Cr-22%, Ni-5.5%, Mo-3.2%, Mn-2%, Si-1%, N-0.16%, P-0.03%, C-0.03% S-0.02%]. Specimens measuring 25 mm × 25 mm × 5 mm were cut using the water jet abrasive cutting method. Then, to get rid of any sharp burrs, these were polished. After meticulously polishing and cleaning the substrate surfaces with acetone, a smooth and uniform surface suitable for applying the coating was achieved. The morphological characteristics and elemental content of DSS 2205 substrate is shown in Fig. 2a. Imperfections and roughness on the substrate surface can influence the bond strength between the coating and substrate [34]. Consequently, the specimens were cleaned with acetone to remove oil marks and cured skin, polished with SiC sheets to 180 grits in order to eliminate oxide scale. The substrate surface was then grit blasted with alumina (grit 60) to obtain a rough surface and enhance the contact area between the coating and substrate before applying the coatings using the D-gun method.

In this study, commercially available Cr_3C_2-NiCr powder with chemical compositions (wt%) of Cr-70.7%, Ni-21.1%, and C-8.2% was utilized. The SEM morphology of the Cr_3C_2-NiCr powders is shown in Fig. 2b. The coating powder has a particle size range of 30–60 μm (mean particle size ≈ 45 μm) was used for coating deposition by the detonation gun (D-gun) spraying process.

The Cr_3C_2-NiCr powders were subsequently applied on DSS 2205 substrate specimens using a commercial D-gun system. The coatings were applied on the top flat surface of the specimen. The cross-sectional views of the coated specimens were analyzed using Scanning Electron Microscope (JEOL, JSM-IT510, Japan) coupled with energy dispersive spectroscopy (EDS). The SEM micrographs along with EDS spectrum were taken with an electron beam energy of 20 keV. Table 1 shows the coating process parameters employed in this study. The spray distances of 170, 180, and 190 mm were selected based on the processing window commonly employed for detonation gun (D-gun) spraying of carbide-based cermet coatings reported in the literature. Within this range, the spray distance has a significant influence on the corrosion performance of the deposited coating. The selected distances therefore provide a systematic basis for evaluating the influence of this critical process parameter while maintaining stable coating deposition conditions [35].

Cross-sectional SEM micrographs were used to determine the coating porosity. The porosity was calculated as the percentage of the segmented pore area relative to the total analyzed coating area. The results are reported as mean ± standard deviation (n = 3). The measured porosity values were 2.84 ± 0.15% at 170 mm, 2.12 ± 0.11% at 180 mm, and 1.38 ± 0.09% at 190 mm.

Table 1
D-gun coating process parameters.

Parameters	Values
Oxygen flow rate (m^3/s)	9.8×10^{-3}
Fuel flow rate (m^3/s)	0.04×10^{-3}
Carrier gas flow rate (m^3/s)	0.013×10^{-3}
Powder feed rate (g/s)	1.5
Spray distance (mm)	170–190
Frequency shots/(sec)	3

2.2. Electrochemical corrosion tests

The electrochemical corrosion behavior of the coated specimens was investigated using electrochemical techniques such as OCP, EIS, Linear Polarization Resistance (LPR) and Potentiodynamic Polarization. The electrochemical measurements were performed with a computer-controlled potentiostat (ZiveSP1, WonATech Co., Ltd. Korea), in 1 M H_2SO_4 corrosive electrolyte solution using a flat three-electrode electrochemical cell with an Ag/AgCl reference electrode, a graphite auxiliary electrode, and the Cr_3C_2-NiCr coated DSS 2205 test specimens as working electrodes. All the electrochemical analyses were carried out at room temperature (27 °C). The area of the specimen exposed to the electrolyte was 1 cm^2.

After exposing the specimen to the electrolyte for equilibration, the OCP was measured for 30 min, with a data point collected for every one second, in line with ASTM C 876. EIS measurements were performed at the OCP with a sinusoidal AC signal in the frequency range of 10 mHz-100 kHz at an amplitude of ±10 mV. The resulting impedance values are displayed as Nyquist plots, Bode plots, and phase angle plots. Linear polarization experiments were conducted on the specimens within a potential window of ±50 mV with respect to OCP. Potentiodynamic polarization measurements were conducted at a rate of 0.166 mV/s, after polarizing the specimens in both anodic and cathodic orientations within a potential window of ±350 mV relative to OCP. Tafel slope analysis and fitting of the data was then carried out to determine the

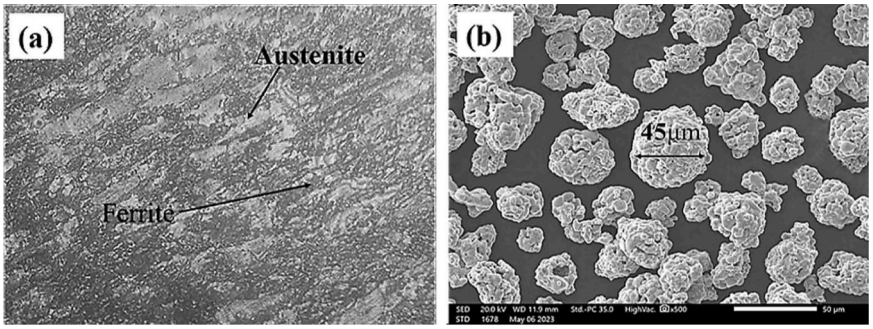


Fig. 2. SEM micrograph (a) DSS 2205 and (b) Cr_3C_2-NiCr powder.

corrosion parameters like corrosion current density (Icorr), corrosion potential (Ecorr), polarisation resistance (Rp), and corrosion rate (CR). After three repetitions, the average value from each trial was selected for examination. The morphology and elemental analysis of the coatings after exposure to the corrosive electrolyte solution was also observed using a SEM coupled with EDS.

3. Results and discussion

3.1. Coated surface analysis

Fig. 3 contains the surface and cross-sectional morphology of the Cr_3C_2-NiCr coating formed on DSS 2205 substrate. The coating thickness was measured from cross-sectional SEM micrographs at five randomly selected locations distributed along the coating cross-section. The coating thickness was measured from cross-sectional SEM micrographs at five randomly selected locations for each spray distance (n = 5). The mean thickness, standard deviation, and measurement range were determined separately for each spray distance. The revised values are 248 ± 9.3 μm for the coating deposited at a spray distance of 170 mm, 251 ± 9.4 μm at 180 mm, and 250 ± 9.4 μm at 190 mm. The corresponding coating-thickness ranges were approximately 239–257 μm, 242–260 μm, and 241–259 μm, respectively. Thus, the reported coating thickness of approximately 250 μm represents an experimentally measured value rather than a nominal thickness. The cross-section reveals that the coating is fully bonded interface to the substrate and does not contain any visible cracks or delamination which confirms the existence of good bonding.

In particular, there is a relatively lower number and small pores in Fig. 3b, more fine pores with dispersed unmelted particles in Fig. 3c, and larger and irregular pores with an increased concentration of unmelted particles in Fig. 3d, which might serve as weak spots in the microstructure. Surface morphology and coating behavior of samples were also studied at various distances of spraying which gave helpful information about the microstructural properties and the distribution of elements. The SEM observations reveal that spray distance has a significant influence on the coating microstructure. The coating deposited at 170 mm exhibits comparatively higher porosity and less uniform splat consolidation, indicating incomplete particle deformation and the presence of interconnected voids. Increasing the spray distance to 180 mm improves particle melting and splat flattening, resulting in a more homogeneous lamellar structure with reduced porosity. The coating deposited at 190 mm exhibits the most compact and continuous microstructure, characterized by fewer micro voids and improved interlamellar cohesion. This improvement is reflected in the reduction of porosity values. Based on these analyses, it was known that the sample sprayed at 190 mm had a more molten structure and high adhesion on DSS 2205 substrate and also the sample sprayed at 190 mm was relatively better in their extent of melting and adhesion as compared to samples sprayed at 180 mm and 170 mm.

3.2. Electrochemical corrosion

3.2.1. Potentiodynamic polarization

The Tafel polarization curve in Fig. 4 shows the electrode potential compared to the OCP, with respect to the logarithm of current density log (i). The measurement is usually done potential range of −350 mV in each side of the OCP and in both the cathodic and anodic branch (oxidation reactions). Under the linear fitting of these branches, anodic and cathodic slopes, βa and βc are obtained. The point of these extrapolated tangents is Ecorr and the resulting point on the current axis is Icorr, which has a quantitative meaning of CR of the specimen.

Fig. 4 indicate the conclusive impact of spray distance on the electrochemical efficiency of thermally sprayed coating. The uncoated specimen exhibited the most vigorous corrosion performance with Ecorr value of about −0.40 V vs. Ag/AgCl and Icorr of 10^{-5} A/cm^2, which determine the tendency of corrosive electrochemical corrosion. In comparison, the overall corrosion current densities and the positive changes in the corrosion potential in all coated specimens were substantively less, which proved that the deposited coatings were protective. There was a systematic increase parameter in the distance to spray with a higher spray distance, i.e., higher Ecorr (about 170 mm to 180 mm) and changes more in Icorr (10^{-5} A/cm^2 to $10^{-5.8}$ A/cm^2) which reflected improved electrochemical stability because of increased

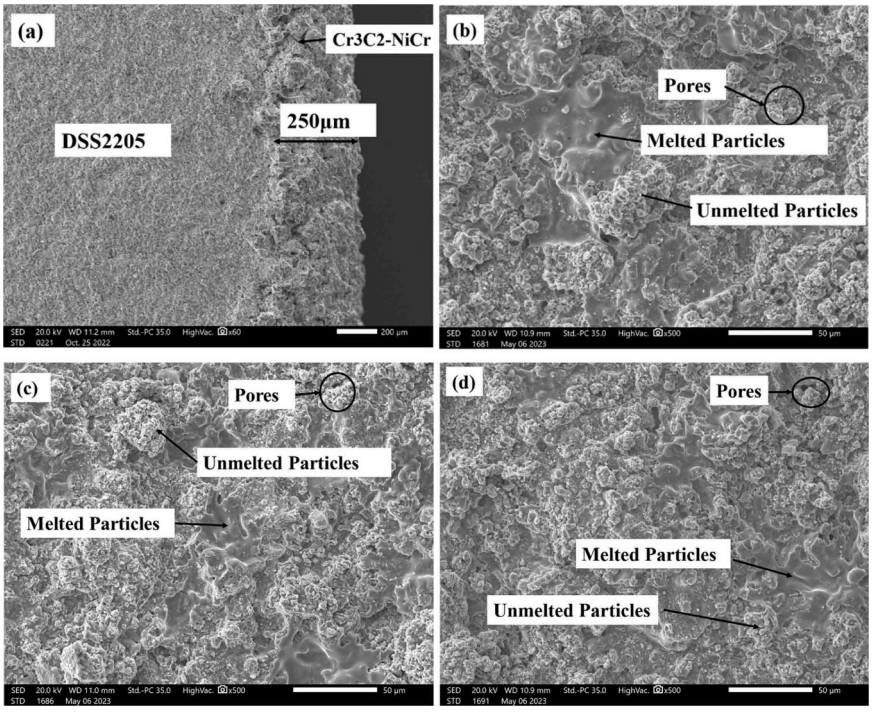


Fig. 3. (a) Cross sectional SEM micrograph of Cr_3C_2-NiCr coated specimens; Morphology of surface at spraying distance of (b) 170 mm, (c) 180 mm, (d) 190 mm.

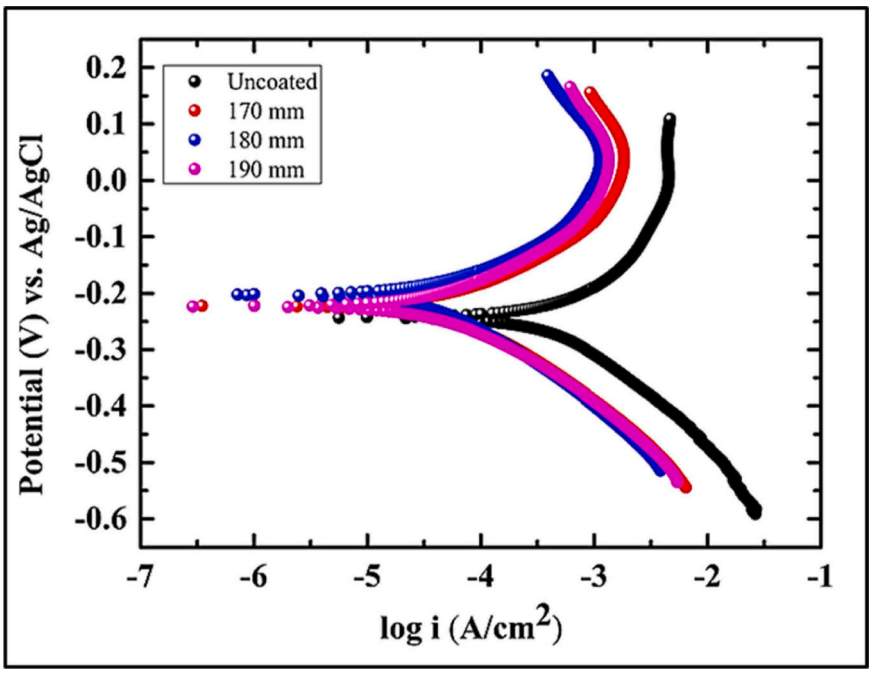


Fig. 4. Potentiodynamic polarization curves of coated and uncoated samples.

spray distance in the positive side of the spectrum. The influence on the spray distance on the particle velocity, splat flattening and porosity can be described by the fact that in the case of optimized distances, the particles will hit the substrate in optimum conditions creating denser and less porous layers preventing the infiltration of electrolytes [35]. Those findings are in line with the outcomes of recent literature on thermal sprays. Jo et al. also found that deposition variables of spray distance and particle velocity had a strong impact on coating density and corrosive properties in stainless steel-silver systems [36]. Liu et al. reported that coating produced at optimum spraying conditions had low i corr values because of reduced defect routes [37]. Moreover, Ali Raza et al. determined that porosity in HVOF coating is reduced at the optimum spray distance, and thus, enhances corrosion resistance [38]. Rakhadilov et al. confirmed that WC-10Co-4Cr coating placed at the same distance of the spray of about 190 mm showed better hardness and wear resistance due to increased microstructural density [39]. Together, these results and literature evidence indicates that the optimum distance of the spray is 190 mm.

The polarization analysis of potentiodynamic in Table 2 shows the effect of spray distance on the corrosion behavior of the thermally sprayed coating in a quantitative way. All electrochemical experiments were performed in triplicate (n = 3) using freshly prepared specimens under identical testing conditions. The Stern–Geary relationship was used to determine corrosion potential (Ecorr), corrosion current density (Icorr), and corrosion rate (CR). The reported electrochemical parameters, including corrosion current density (Icorr), polarization resistance (Rp), and CR, are presented as, mean ± standard deviation in Table 2. The bare sample had the worst performance and its values of Ecorr = −0.2418 ± 0.0121 V, Icorr = (2.43 ± 0.12) × 10^{-4} A/cm^2, Rp = 90.06 ± 4.50 Ω.cm^2 and CR = 2.600 ± 0.130 mmpy indicating its extreme susceptibility to degradation. Conversely, electrochemical stability of all the coated samples was greatly enhanced through indicating more noble corrosion potentials, smaller current densities, stronger polarization resistance and lowering CR. The coating increased the Ecorr = −0.2215 ± 0.0111 V, reduced Icorr = (2.38 ± 0.12) × 10^{-5} A/cm^2 at 170 mm and Rp = 380.22 ± 19.01 Ω.cm^2 and CR = 0.254 ± 0.013 mmpy. The best performance was at 180 mm (Icorr = (1.40 ± 0.07) × 10^{-5} A/cm^2, Ecorr = −0.2213 ± 0.0111 V, Rp = 647.51 ± 32.38 Ω.cm^2, CR = 0.150 ± 0.008 mmpy) and the best performance occurred at 190 mm, Icorr = (1.06 ± 0.05) × 10^{-5} A/cm^2, Ecorr = −0.2029 ± 0.0101 V, Rp = 1667.52 ± 83.38 Ω.cm^2, and CR decreased to 0.113 ± 0.006 mmpy.

Table 2
Tafel fitted parameters for specimens exposed in 1 M H_2SO_4 solution.

	Uncoated	170 mm	180 mm	190 mm
βa (V/dec)	0.0914 ± 0.0046	0.0394 ± 0.0020	0.0386 ± 0.0019	0.0773 ± 0.0039
βc (V/dec)	0.1124 ± 0.0056	0.0442 ± 0.0022	0.0455 ± 0.0023	0.0859 ± 0.0043
Icorr (A/cm^2)	(2.43 ± 0.12) × 10^{-4}	(2.38 ± 0.12) × 10^{-5}	(1.40 ± 0.07) × 10^{-5}	(1.06 ± 0.05) × 10^{-5}
Ecorr (V)	−0.2418 ± 0.0121	−0.2215 ± 0.0111	−0.2213 ± 0.0111	−0.2029 ± 0.0101
Rp (Ω·cm^2)	90.06 ± 4.50	380.22 ± 19.01	647.51 ± 32.38	1667.52 ± 83.38
CR (mm/year)	2.600 ± 0.130	0.254 ± 0.013	0.150 ± 0.008	0.113 ± 0.006

The trends validate the fact that the increase of a spray distance in the selected ranges increases coating integrity through the encouragement of denser microstructures with less active defect sites, which ensures enhanced protection against electrolyte permeation as a barrier. The continuous growth of Rp and CR versus the spray distance leads to the finding that the 190 mm condition gave the most protective coating. This finding is similar to previous research, in which optimized spray distances were demonstrated to play a role in decrease of porosity and oxidation, resulting in a lower Icorr and higher noble Ecorr value. In addition, it was further noted that deposition parameters, especially the spray distance and velocity of the particle play vital roles in coating densities and electrochemical stability, whereas Avram et al. found comparable enhancement in the low-carbon steel coverings in simulated PEMFC settings [40].

Overall, the Tafel analysis offers major understanding on the mechanism of corrosion using Ecorr, Icorr, Rp, and CR. The conditions with the best electrochemical parameters were 190 mm spray distance followed by 180 mm, 170 mm, and the worst was the uncoated substrate. These results determine the spray distance to be a critical processing variable in maximizing thermal spray finishes and show that there is a high relationship between deposition control, microstructural quality

and corrosion resistance.

3.2.2. Electrochemical impedance spectroscopy

EIS is a popular method used to measure corrosion behaviour through the Bode and Nyquist plots, which gives information about the electrochemical characteristics. The measurements of EIS were made within the frequency range of 10 kHz to 100 kHz. The Nyquist plots (Fig. 5a) indicate a drastic effect on the real-axis intercept and the intuitive radius of a semicircle in coated samples as opposed to the uncoated substrate. This tendency means that the polarization resistance increases highly when the coating is applied, i.e. the coating is an efficient barrier, which augments the resistance to delivering any charge and ion transportation at low frequencies. The impedance of the coated samples at low frequencies increased significantly with increasing spray distance. Correspondingly, the diameter of the Nyquist semicircle also enlarged as the spray distance increased. This behavior indicates an improvement in coating barrier properties and enhanced resistance to electrolyte penetration through pores. The larger semicircle diameter reflects higher Rp, which is characteristic of coating systems exhibiting superior corrosion protection performance [41,42].

The Nyquist results are supported by the Bode magnitude plot (Fig. 5b). The impedance values of the coated samples at low frequencies (0.011 Hz) are so large compared to the impedance of the uncoated surface- determined to be approximately 10–100 times higher. The coating with the largest impedance at low frequencies is that of the largest coated samples, and most likely the most stable. Bode plot indicates effective control of lower frequency by the coating (high impedance) and high frequency by the solution or electric resistance (low impedance) quite evidently. To do this practically, the impedance at very low frequency (e.g. 0.01 Hz or 10 MHz) is typically reported to indicate the performance of the coating in protecting the surface [43].

In Fig. 5c, it can be observed that the coated samples have a strong peak in the frequency range of 1–2 Hz as indicated by the phase-angle spectra. The wide range of phase angle of the coated samples is high, about 60–70°. With the uncoated substrate, on the other hand, the phase response is a lot smaller with a lone great deal less around 35–40°, and has a broader and less strong peak.

A substantial and sharp phase peak is one characteristic of a desirable coating, and denotes desirable capacitive (barrier) characteristics at medium frequencies. The phase peak location varies a bit with the spraying distance, and this indicates that the coating resistance and/or capacitance varies. The coated specimens exhibit a dominant phase-angle response over the investigated frequency range. However, the presence of a single prominent phase-angle maximum does not necessarily imply a single electrochemical time constant. [44].

Fig. 5d demonstrates that the coated surfaces stabilize at a little more positive (less negative) potentials whereas the bare substrate swings to much more negative values. The bare sample has an insignificant time to reach a low potential of approximately −0.30 V to −0.35 V. On the contrary, the coated samples are maintained at around −0.10 V to −0.15 V and very slight variation towards the negative side is observed in the test. Higher positive (nobler) open-circuit potential of the coated samples suggests that the coating isolates the metal by inhibiting active corrosive ionic contact, and also decreasing active currents caused by corrosion. The gradual movement of the negative potential implies low ability to absorb water and slow exposing of the metal with the help of coating pores. Open circuit potential data give convenient support data and is to be integrated with EIS data and surface observations [45,46].

The equivalent electrical circuit depicted in Fig. 6 of the thermally sprayed coatings. Solution resistance (Rs), coating resistance (Rcoat),

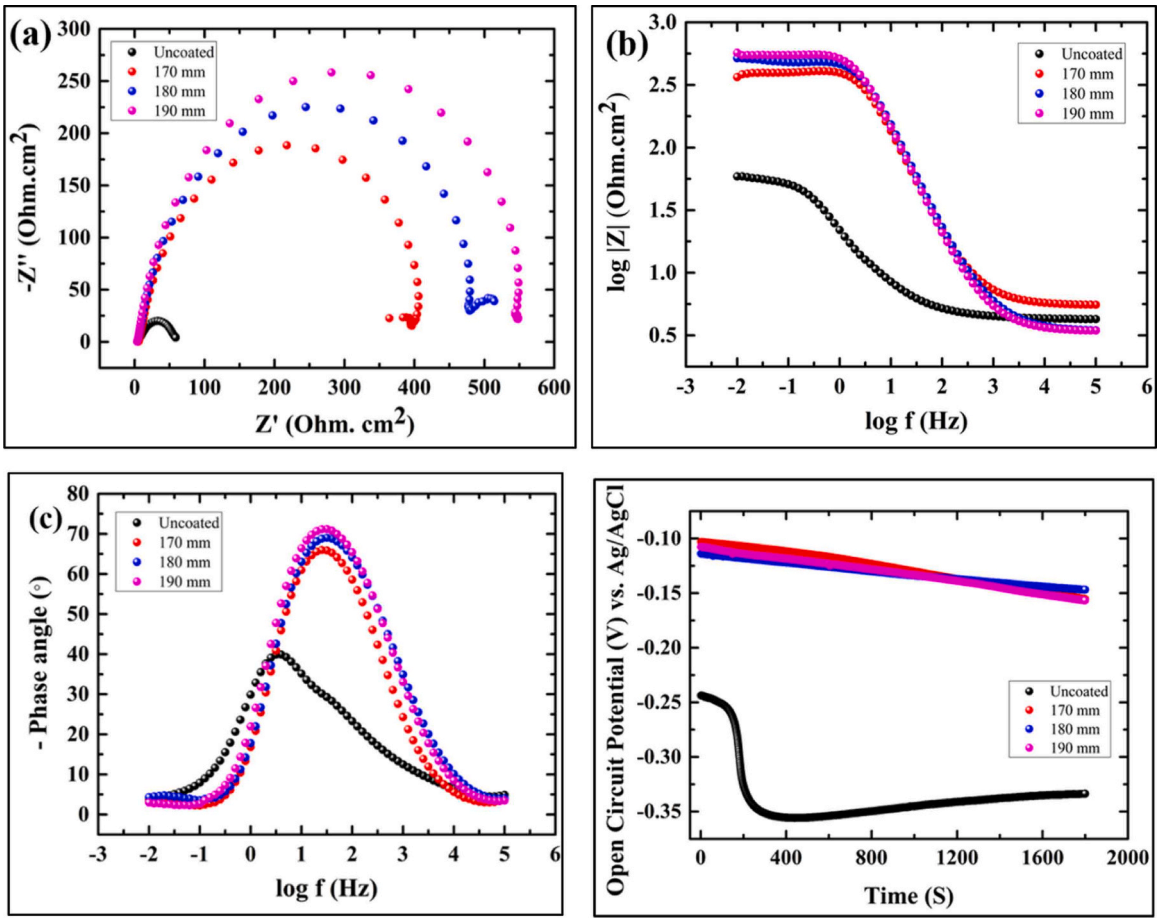


Fig. 5. Electrochemical impedance spectroscopy (a) Nyquist plot, (b) Bode plot, (c) Phase angle plot, (d) Open circuit plot.

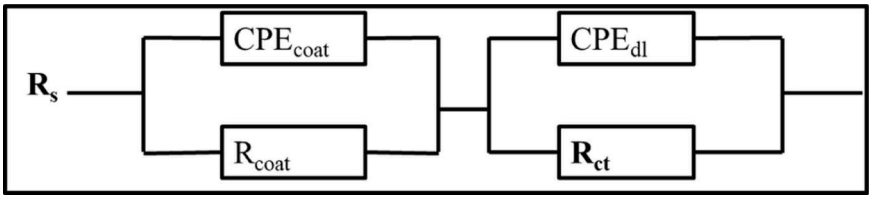


Fig. 6. Equivalent circuit.

coating constant phase element (CPEcoat), charge-transfer resistance (Rct), and double-layer constant phase element (CPEdl) make up the suggested circuit.

Table 3 provides a summary of the fitted impedance parameters. During the electrochemical experiments, Rs stayed almost consistent for every specimen, indicating that the electrolyte conditions were the same. On the other hand, when the spray distance rose, Rcoat and Rct both gradually increased, suggesting improved barrier properties associated with a denser coating microstructure. suggesting the development of a denser coating against electrolyte penetration. Due to its compact microstructure and decreased interconnected porosity, the coating deposited at a spray distance of 190 mm demonstrates the maximum corrosion resistance, according to these measurements, which are in excellent agreement with the Nyquist and Bode plots.

3.2.3. *Linear polarization resistance and potentiodynamic polarization*

The polarization resistance (Rp) was determined independently using the Linear Polarization Resistance (LPR) technique, and the obtained values were used to evaluate the electrochemical barrier performance of the coatings. Fig. 7 demonstrates a significant improvement in the electrochemical protection by the Cr_3C_2–NiCr coatings. All the coated specimens showed significantly higher Rp values and lower CR, while uncoated substrate exhibited the lowest Rp and the highest CR. Two significant patterns are apparent: (i) the coating substantially reduces CR in comparison with the uncoated specimen, and (ii) As the spray distance increased from 170 to 190 mm, a steady increase in polarisation resistance was observed.

The microstructural characteristics of thermally sprayed coatings significantly influence their electrochemical behaviour, including coating porosity, inter-lamellar bonding, oxide content and thickness, which are sensitive to process standoff distance as well as delivered thermal/kinetic energy to the powder particles during transit. Several recent studies have reported that the degree of change in a spray distance influences (a) particle temperature and velocity upon impact, (b) level of particle deformation, splat flattening, (c) oxidation degree in the in-flight particle and, (d) porosity and connectivity between the layers, which determines the electrolyte penetration and resistance to corrosion [47–51].

3.3. *Surface characterization*

The post-corrosion surface morphologies of the coatings sprayed at various spray distances after electrochemical testing are shown in Fig. 8. At a spray distance of 170 mm the surface is marked by discrete, irregular nodules and partially exposed matrix between sites of corrosion, shallow pits and sharp ridges are observed across the arrows, which means that initial local deterioration of the passive film and early dissolution are taking place. The corresponding EDS spectrum reveals oxygen enrichment along with nickel and chromium. At 180 mm, these nodular corrosion develops to larger, coalesced clusters and the inter-nodule distance is reduced, which is an indication of further dissolution of metals and rearrangement of the oxides to form an increasingly porous, interconnected corrosion -product layer. At 190 mm the topography is rather dominated by a cauliflower-like morphology, indicating the formation of a relatively thick multilayer corrosion-product layer. EDS reveals still high levels of Cr and O, and limited amounts of Ni, indicating that the scale is Cr-enriched, and surface oxide formation has been concentrated through the selective dissolution of the underlying matrix. Taken together, the series of steps between (a) to (c) is given by the progressive breakdown of the passive-film by passive oxide, the formation and growth of the initial pit followed by transformation to a larger oxide layer rather than uniform passive film dissolution.

The corresponding EDS spectrum reveals enrichment of oxygen along with nickel and chromium The same morphologies (patchy nodules that develop into coalesced porous oxide layers) have been observed in recent investigations of duplex and Ni-Cr finishes and welded stainless steel where it is attributed that morphological evolution may originate at localized sites of chloride breakdown and subsequent rapid oxide nucleation and growth. These investigations also stress that the morphology and protective nature of the scale are highly variable with the local composition, microstructure and the degree of exposure, that could be observed in the change between individual pits to a nearly continuous oxide layer [52].

Thermally sprayed nichrome coatings on DSS substrates have been reported to exhibit similar phenomena in previous studies. SEM/EDS analyses have been used to correlate coating microstructure and coverage with electrochemical corrosion behavior. Previous optimization studies and corrosion measurements indicate that incomplete or porous coating layers promote localized corrosion and oxidation, consistent with the observations in the present work [53]. Furthermore, Kuruvila et al. demonstrated that processing parameters and coating thickness significantly influences the stability of Cr-rich passive phases. These findings align with our interpretation that the observed changes arise from the gradual degradation of a protective surface state and the subsequent formation of Cr-rich corrosion products [54].

Table 3
Equivalent parameters for EIS.

Sample	Rs ($\Omega\cdot cm^2$)	Rcoat ($\Omega\cdot cm^2$)	CPEcoat ($F\cdot cm^{-2}\cdot s^{n-1}$)	Rct ($\Omega\cdot cm^2$)	CPEdl ($F\cdot cm^{-2}\cdot s^{n-1}$)
170 mm	11.8	3.45×10^3	8.90×10^{-5}	2.42×10^4	1.85×10^{-4}
180 mm	12.1	5.96×10^3	6.75×10^{-5}	4.81×10^4	1.12×10^{-4}
190 mm	12.4	9.84×10^3	4.21×10^{-5}	8.37×10^4	6.75×10^{-5}

4. Limitations and future scope

Although the present investigation provides valuable insights into the influence of spray distance on the microstructural evolution and corrosion performance of Cr_3C_2-NiCr coatings, certain limitations must be acknowledged. The study was restricted to a single feedstock composition and a fixed range of spray distances, which may limit the general applicability of the findings to other carbide–metal systems or broader processing conditions. Furthermore, the corrosion evaluation was primarily based on short-term electrochemical testing under controlled laboratory conditions, which may not fully represent long-term service exposure or high-temperature operating environments encountered in industrial service conditions. A quantitative correlation between corrosion behavior and critical mechanical properties such as hardness, adhesion strength, and wear resistance was not established. In addition, advanced characterization techniques such as X-ray

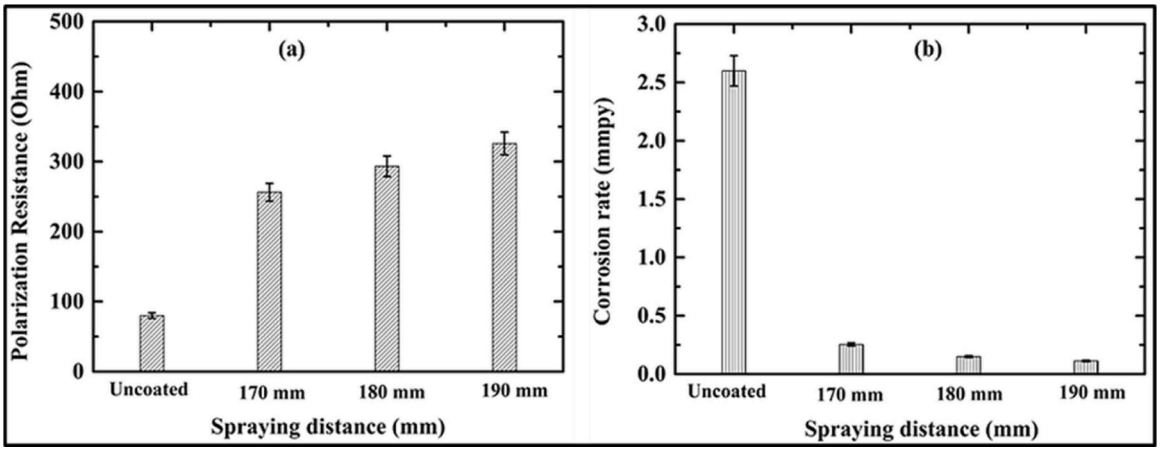


Fig. 7. CR of the coated samples deposited at different spray distances compared with the uncoated substrate using LPR.

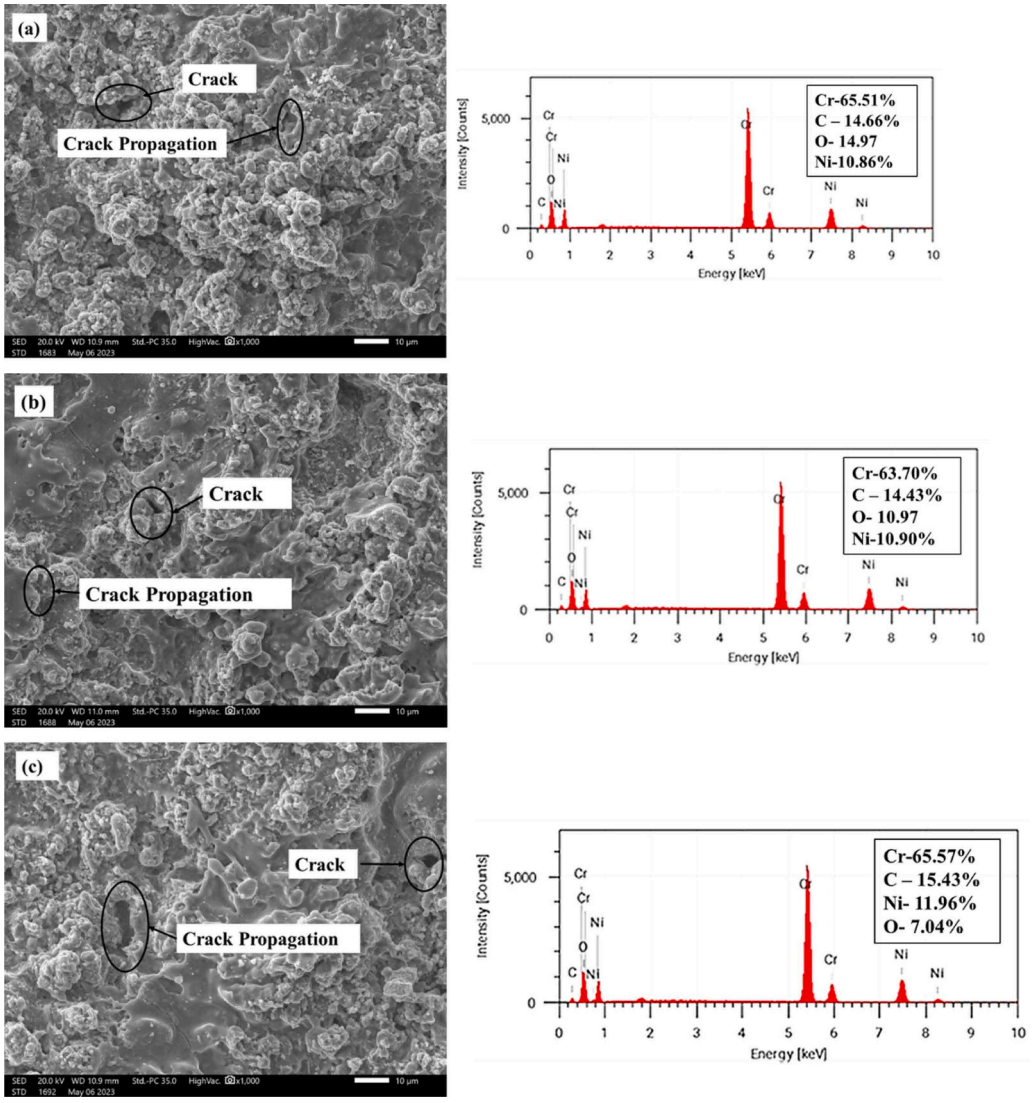


Fig. 8. Surface morphology after corrosion (a) 170 mm, (b) 180 mm, (c) 190 mm.

photoelectron spectroscopy (XPS) and transmission electron microscopy (TEM) were not employed, thereby limiting a comprehensive understanding of passive film chemistry, oxide scale evolution, and inter-lamellar bonding mechanisms at the nanoscale.

Future investigations should expand upon the present work by exploring additional detonation gun process parameters, including detonation frequency, oxygen–fuel ratio, and substrate preheating temperature, in order to optimize coating microstructure, architecture

and functional performance. Long-term immersion testing and cyclic corrosion studies under simulated marine and industrial environments are recommended to provide a more realistic evaluation of coating durability and service life. The incorporation of advanced surface analytical techniques such as XPS and focused ion beam–TEM (FIB-TEM) would enable deeper insight into nanoscale passive film stability, interfacial bonding mechanisms, and coating-substrate interactions. Future studies should also incorporate advanced characterization techniques such as XRD, XPS, and TEM/FIB-TEM to correlate phase constitution, passive film stability, and interfacial microstructure with electrochemical behaviour. Finally, integrating experimental investigations with first-principles Density Functional Theory, Molecular Dynamics simulations, and machine learning-assisted process–structure–property modelling would provide a comprehensive multiscale understanding of corrosion mechanisms and accelerate the optimization and industrial implementation of high-performance Cr_3C_2–25NiCr protective coatings.

5. Conclusion

The systematic investigation on the influence of spray distance on the microstructural development and corrosion behavior of Cr_3C_2-NiCr coatings deposited on 2205 duplex stainless steel using the detonation gun (D-gun) thermal spray process has the following conclusions.

- The spray distance significantly influenced the coating microstructure and electrochemical performance. Increasing the spray distance promoted the formation of dense, compact, and well-bonded Cr_3C_2–25NiCr coatings with reduced porosity, improved interlamellar cohesion, and no visible cracks or delamination, thereby enhancing corrosion resistance and establishing a clear processing–microstructure–corrosion relationship.
- Among the investigated spray distances, the coating deposited at 190 mm exhibited the most refined and compact microstructure, characterized by lower porosity, improved interlamellar cohesion, and more homogeneous lamellar stacking, resulting in superior coating integrity.
- Electrochemical investigations (OCP, EIS, and potentiodynamic polarization) confirmed that all Cr_3C_2–25NiCr coatings enhanced the corrosion resistance of DSS 2205 compared with the uncoated substrate. The coating deposited at 190 mm demonstrated the best corrosion performance, exhibiting the most noble corrosion potential ($E_{corr} = 0.2029 \pm 0.0101$ V), the lowest corrosion current density ($I_{corr} = (1.06 \pm 0.05) \times 10^{-5}$A cm^{-2}), the highest polarization resistance ($R_p = 1667.52\ \Omega{\cdot}cm^2$), and the lowest corrosion rate, thereby identifying 190 mm as the optimum spray distance for corrosion protection under the investigated conditions
- SEM/EDS analyses revealed that localized corrosion features and Cr- and O-enriched surface regions on the coated specimens, effectively reduced the density of active corrosion sites and limited electrolyte ingress.
- The increase in spray distance promoted higher effective particle velocity and improved splat flattening, resulting in denser coatings with fewer defects and superior electrochemical stability.
- From an engineering perspective, spray distance is identified as a critical process parameter for optimizing D-gun coatings, enabling the development of durable corrosion-resistant surfaces for equipment operating in aggressive acidic environments of silicon-processing industries.

CRediT authorship contribution statement

Roshan Kuruvila: Writing – original draft, Investigation, Conceptualization. **Mebin T. Kuruvila:** Methodology, Formal analysis, Data curation. **Manu Harilal:** Validation, Software, Methodology, Formal analysis. **S. Thirumalai Kumaran:** Writing – review & editing, Supervision, Resources, Methodology, Conceptualization.

Ethics approval

We comply with ethical standards. We provide our consent to take part.

Consent to participate/publication

The authors provide consent to participate/publication.

Funding

This research received no specific grant from any funding agency in the public, commercial, or not-for-profit sectors.

Declaration of Competing Interest

The authors declare that they have no known competing financial interests or personal relationships that could have appeared to influence the work reported in this paper.

Data availability

Data will be made available on request.

References

[1] H.M.H. Farh, M.E.A.B. Seghier, T. Zayed, A comprehensive review of corrosion protection and control techniques for metallic pipelines, Eng. Fail. Anal. 143 (2023) 106885.
[2] R. Kuruvila, T.K. Sundaresan, F. Ahmed, U. Marimuthu, Electrochemical corrosion behavior of thermally sprayed nichrome coating on duplex stainless steel, J. Test. Eval. 52 (1) (2024) 203–217.
[3] A. Zubail, A. Traidia, M. Masulli, K. Vatopoulos, T. Villette, I. Taie, Carbon and energy footprint of nonmetallic composite pipes in onshore oil and gas flow lines, J. Clean. Prod. 305 (2021) 127150.
[4] H. Niazi, R. Eadie, W. Chen, H. Zhang, High pH stress corrosion cracking initiation and crack evolution in buried steel pipelines: a review, Eng. Fail. Anal. 120 (2021) 105013.
[5] H. Tan, Y. Jiang, B. Deng, T. Sun, J. Xu, J. Li, Effect of annealing temperature on the pitting corrosion resistance of super duplex stainless steel UNS S32750, Mater. Charact. 60 (9) (2009) 1049–1054.
[6] P.J. Antony, S. Chongdar, P. Kumar, R. Raman, Corrosion of 2205 duplex stainless steel in chloride medium containing sulfate-reducing bacteria, Electrochim. Acta 52 (12) (2007) 3985–3994.
[7] P. Kangas, G.C. Chai, Use of advanced austenitic and duplex stainless steels for applications in Oil & Gas and Process industry, Adv. Mater. Res. 794 (2013) 645–669.
[8] T. Zhang, Y. Zhao, B. Dong, X. Li, Corrosion behaviour of 2205 DSS in the artificial industrial-marine environment, Corros. Eng. Sci. Technol. 56 (1) (2021) 22–34.
[9] R. Kuruvila, S.T. Kumaran, M.A. Khan, M. Uthayakumar, Optimization of solid particle erosion of 2205 duplex stainless steel under air jet using Taguchi method, IOP Conf. Ser.: Mater. Sci. Eng. 1057 (1) (2021) 012073. IOP Publishing.
[10] R. Kuruvila, S. Thirumalai Kumaran, R. Kurniawan, Optimization of solid particle erosion behavior of thermally sprayed nichrome on duplex stainless steel, Int. J. Interact. Des. Manuf. (IJIDeM) 18 (7) (2024) 5027–5041.
[11] H. Tian, X. Cheng, Y. Wang, C. Dong, X. Li, Effect of Mo on interaction between α/γ phases of duplex stainless steel, Electrochim. Acta 267 (2018) 255–268.
[12] D.S. Pamuji, M.L. Hakim, Investigation of mechanical, microstructure, and corrosion properties of duplex stainless steel joint for natural gas processing facilities, IOP Conf. Ser.: Earth Environ. Sci. 1151 (1) (2023) 012056. IOP Publishing.
[13] R. Kuruvila, S.T. Kumaran, M.A. Khan, Solid particle erosion behavior of nichrome coated duplex stainless steel, Int. J. Adv. Technol. Eng. Explor. 9 (97) (2022) 1741.
[14] Y. Hou, Y. Nakamori, K. Kadoi, H. Inoue, H. Baba, Initiation mechanism of pitting corrosion in weld heat affected zone of duplex stainless steel, Corros. Sci. 201 (2022) 110278.
[15] M. Conradi, P.M. Schön, A. Kocijan, M. Jenko, G.J. Vancso, Surface analysis of localized corrosion of austenitic 316L and duplex 2205 stainless steels in simulated body solutions, Mater. Chem. Phys. 130 (1-2) (2011) 708–713.
[16] L.V. Jinlong, W. Zhuqing, L. Tongxiang, S. Ken, M. Hideo, Enhancing the corrosion resistance of the 2205 duplex stainless steel bipolar plates in PEMFCs environment by surface enriched molybdenum, Results Phys. 7 (2017) 3459–3464.
[17] D. Kong, C. Dong, X. Ni, L. Zhang, J. Yao, C. Man, X. Cheng, K. Xiao, X. Li, Mechanical properties and corrosion behavior of selective laser melted 316L

stainless steel after different heat treatment processes, J. Mater. Sci. Technol. 35 (7) (2019) 1499–1507.
[18] Q. Cheng, B. Tao, L. Song, W. Zhang, X. Liu, W. Li, B. Hou, Q. Liu, Corrosion behaviour of Q235B carbon steel in sediment water from crude oil, Corros. Sci. 111 (2016) 61–71.
[19] X. Cheng, Y. Wang, C. Dong, X. Li, The beneficial galvanic effect of the constituent phases in 2205 duplex stainless steel on the passive films formed in a 3.5% NaCl solution, Corros. Sci. 134 (2018) 122–130.
[20] R. Kuruvila, R. Jayakrishnan, Corrosion measurement of thermally sprayed carbide coatings on stainless steel pipes, Results Surf. Interfaces 17 (2024) 100320.
[21] Y. Gong, C. Xiao, S. Hu, Y. Zhou, C. Li, B. Yang, J. Zhang, G. Zhang, Investigation on microstructure and properties of cold-sprayed Ni-Mo-Al2O3 composite coating, Coatings 14 (2) (2024) 205.
[22] V.M. Gopinath, S. Arulvel, A review on the steels, alloys/high entropy alloys, composites and coatings used in high temperature wear applications, Mater. Today. Proc. 43 (2021) 817–823.
[23] S. Kant, Introduction: Thermal Spray Coatings and their Historical Developments. Thermal Spray Coatings: Materials, Techniques & Applications, Bentham Science Publishers, 2024, pp. 1–24.
[24] V. Gupta, Overview of the HVOF (High Velocity Oxy Fuel) thermal spray coating process used to combat hot corrosion of coal–fired boiler parts, Adv. Mater. Technol. (2024) 1.
[25] H. Du, W. Hua, J. Liu, J. Gong, C. Sun, L. Wen, Influence of process variables on the qualities of detonation gun sprayed WC–Co coatings, Mater. Sci. Eng. A 408 (1-2) (2005) 202–210.
[26] C. Tan, K. Krishnan, N.K. Elumalai, Corrosion behaviour of heat-treated cold spray nickel chromium/chromium carbides, Metals 14 (10) (2024) 1153.
[27] T. Arunnellaiappan, S. Baskaran, S. Arun, R. Prithivirajan, Corrosion behaviour of detonation gun sprayed cermet coatings on AA5083, Surf. Eng. 37 (2) (2021) 263–270.
[28] R.J.K. Wood, B.G. Mellor, M.L. Binfield, Sand erosion performance of detonation gun applied tungsten carbide/cobalt-chromium coatings, Wear 211 (1) (1997) 70–83.
[29] A. Meghwal, S. Matthews, H. Howse, C.C. Berndt, A.S.M. Ang, Steam and air oxidation behaviour of thermal spray chromium carbide-based composite coatings, Int. J. Refract. Met. Hard Mater. 111 (2023) 106088.
[30] S. Kamal, R. Jayaganthan, S. Prakash, S. Kumar, Hot corrosion behavior of detonation gun sprayed Cr3C2–NiCr coatings on Ni and Fe-based superalloys in Na2SO4–60% V2O5 environment at 900°C, J. Alloy. Compd. 463 (1-2) (2008) 358–372.
[31] A.R. Govande, A. Chandak, B.R. Sunil, R. Dumpala, Carbide-based thermal spray coatings: a review on performance characteristics and post-treatment, Int. J. Refract. Met. Hard Mater. 103 (2022) 105772.
[32] D. Mudgal, S. Singh, S. Prakash, Hot corrosion behavior of bare, Cr3C2-(NiCr) and Cr_3C_2-(NiCr)+ 0.2 wt% Zr coated SuperNi 718 at 900 °C, J. Mater. Eng. Perform. 24 (1) (2015) 1–15.
[33] P. Saravanan, V. Selvarajan, D.S. Rao, S.V. Joshi, G. Sundararajan, Influence of process variables on the quality of detonation gun sprayed alumina coatings, Surf. Coat. Technol. 123 (1) (2000) 44–54.
[34] A. Günen, B. Soylu, Ö. Karakaş, Titanium carbide coating to improve surface characteristic, wear and corrosion resistance of spheroidal graphite cast irons, Surf. Coat. Technol. 437 (2022) 128280.
[35] T. Ghara, P.P. Bandyopadhyay, Splat shape and pore size distribution in plasma sprayed alumina coating at various in-flight particle conditions, J. Therm. Spray. Technol. 32 (6) (2023) 1879–1892.
[36] H. Jo, J.W. Ok, Y.S. Lee, S. Lee, Y. Je, S. Kim, S. Kim, J. Park, J. Hong, T. Lee, B. H. Shin, Impact of Ag coating thickness on the electrochemical behavior of super duplex stainless steel SAF2507 for enhanced Li-ion battery cases, Crystals 15 (1) (2025) 62.
[37] M. Liu, Z. Tan, Y. Zhao, H. Wang, S. Zhang, R. Ma, T. Jiang, Z. Ma, N. Zhong, W. Li, Optimization of spray parameters and corrosion properties of plasma-sprayed Cr2O3 coatings using response surface methodology, Crystals 15 (4) (2025) 377.
[38] A. Raza, F. Ahmad, T.M. Badri, M.R. Raza, K. Malik, An influence of oxygen flow rate and spray distance on the porosity of HVOF coating and its effects on corrosion—a review, Materials 15 (18) (2022) 6329.
[39] B. Rakhadilov, N. Muktanova, D. Kakimzhanov, M. Adilkanova, S. Kurbanbekov, S. Abdulina, Influence of varying the spraying distance on the structural-phase state and mechanotribological properties of 86WC-10Co-4Cr-based coatings obtained by the HVOF method, Coatings 14 (3) (2024) 264.
[40] D.N. Avram, C.M. Davidescu, I. Hulka, M.L. Dan, E.M. Stanciu, A. Pascu, J. C. Mirza-Rosca, Corrosion behavior of coated low carbon steel in a simulated PEMFC environment, Materials 16 (8) (2023) 3056.
[41] R. Kuruvila, S.T. Kumaran, M.A. Khan, Optimization of erosion–corrosion behavior of nichrome coated 2205 duplex stainless steel using grey relational analysis, Surf. Rev. Lett. 29 (07) (2022) 2250087.
[42] J. Zhang, S. Wang, K. Ono, Electrochemical impedance spectroscopy. Microscopy and Microanalysis for Lithium-Ion Batteries, CRC Press, 2023, pp. 301–350.
[43] D. Loveday, P. Peterson, B. Rodgers, Evaluation of organic coatings with electrochemical impedance spectroscopy, JCT Coat. Tech. 8 (2004) 46–52.
[44] L. Zhang, Y. Dai, C. Li, Y. Dang, R. Zheng, Z. Wang, Y. Wang, Y. Cui, H. Arandiyan, Z. Shao, H. Sun, Recent advances in electrochemical impedance spectroscopy for solid-state batteries, Energy Storage Mater. 69 (2024) 103378.
[45] A. Trentin, A. Pakseresht, A. Duran, Y. Castro, D. Galusek, Electrochemical characterization of polymeric coatings for corrosion protection: a review of advances and perspectives, Polymers 14 (12) (2022) 2306.
[46] R. Kuruvila, S. Thirumalai Kumaran, A. Varghese, S. Suresh Kumar, M. Uthayakumar, Comparison of electrochemical corrosion behavior of chromium carbide and tungsten carbide on DSS2205 by atmospheric plasma coating, Surf. Rev. Lett. (2025) 2550172.
[47] Y. Han, Y. Zhang, H. Jing, Z. Gao, L. Xu, Z. Zhang, L. Zhao, Microstructure and corrosion studies on different zones of super duplex stainless steel UNS S32750 weldment, Front. Mater. 7 (2020) 251.
[48] K. Du, C. Song, M. Liu, T. Liu, K. Wen, H. Liao, C. Yang, Preparation of yttria-stabilized zirconia electrolyte via atmospheric plasma spraying for metal-supported solid oxide fuel cells, Int. J. Hydrogen Energy 50 (2024) 1133–1141.
[49] W.L. Chen, M. Liu, X.L. Xiao, X. Zhang, Effect of spray distance on the microstructure and high temperature oxidation resistance of plasma spray-physical vapor deposition 7YSZ thermal barrier coating, Mater. Sci. Forum 1035 (2021) 511–520. Trans Tech Publications Ltd.
[50] L. Gui, B. Wang, R. Cai, Z. Yu, M. Liu, Q. Zhu, Y. Xie, S. Liu, A. Killinger, Prediction of in-flight particle properties and mechanical performances of HVOF-sprayed NiCr–Cr3C2 coatings based on a hierarchical neural network, Materials 16 (18) (2023) 6279.
[51] A. Fernández Roiz, J.A. Moreno, G. Jorde Cerezo, J. Solano, Analysis of the relationship between APS thermal spray parameters of Ni5Al particles and coating characteristics, Coatings 13 (9) (2023) 1564.
[52] W. Tillmann, O. Khalil, I. Baumann, Influence of direct splat-affecting parameters on the splat-type distribution, porosity, and density of segmentation cracks in plasma-sprayed YSZ coatings, J. Therm. Spray. Technol. 30 (4) (2021) 1015–1027.
[53] R. Kuruvila, S. Thirumalai Kumaran, Optimization of erosion resistance in duplex stainless steel DSS2205 for enhanced performance, Can. Metall. Q. 65 (1) (2026) 703–717.
[54] R. Kuruvila, T. Thomas, T.K. S, F. Ahmed, Data-driven erosion-corrosion mitigation of 2205 duplex stainless steel, J. Adhes. Sci. Technol. (2025) 1–19.